Evaluating the accuracy of C- and X-band weather radars and their application for stream flow simulation

N. K. Shrestha, T. Goormans and P. Willems

ABSTRACT

This paper investigates the accuracy of rainfall estimates from C- and X-band weather radars and their application for stream flow simulation. Different adjustment procedures are applied to raw radar estimates using gauge readings from a network of 12 raingauges. The stream flow is simulated for the 48.17 km^2 Molenbeek/Parkbeek catchment located in the Flemish region of Belgium based on a lumped conceptual model. Results showed that raw radar estimates can be greatly improved using adjustment procedures. The gauge-radar residuals however, remain large even after adjustments. The adjusted X-band radar estimates are observed to be better estimates than corresponding C-band estimates. Their application for stream flow simulation showed that raingauges and radars can simulate spatially more uniform winter storms with almost the same accuracy, whereas differences are more evident on summer events.

Key words | lumped conceptual model, stream flow simulation, weather radar raingauges

N. K. Shrestha (corresponding author)
T. Goormans
P. Willems
Hydraulics Laboratory,
Department of Civil Engineering,
University of Leuven,
3000 Leuven,
Belgium
E-mail: *nashrest@vub.ac.be*

N. K. Shrestha
P. Willems
Department of Hydrology & Hydraulic Engineering,
Vrije Universiteit Brussel,
Pleinlaan 2,
1050 Brussels,
Belgium

INTRODUCTION

Use of simulation models to understand, design, forecast and manage water resources is a common practice. These models naturally require rainfall as a primary input (Segond *et al.* 2007; Goormans & Willems 2008; Velasco-Forero *et al.* 2008; Goormans 2011). The quality of model-derived information highly depends on the accuracy of the spatial and temporal quantitative and qualitative measurement/estimation of rainfall over the model domain (Sempere-Torres *et al.* 2000; Uijlenhoet 2001). When few data of adequate spatial and temporal resolution are available, rainfall is assumed to be uniformly distributed over the catchment (Vaes *et al.* 2005). Such ignorance of the spatial rainfall variability is in many current modelling applications, the major source of uncertainty in model-derived information (Willems 2001; Willems & Berlamont 2002). Traditionally, hydrologists seem to be more interested in the development of sophisticated hydrological models or local models that suit local surface and subsurface conditions than to investigate space–time variability of rainfall and subsequent development of improved techniques to capture that variability (Berne *et al.* 2005). Rather, better understanding and accurate quantitative estimation of the rainfall input is required for improving the accuracy of simulated events in such models (Goudenhoofdt & Delobbe 2009). The advantage of using a finer resolution (spatial and temporal) rainfall field in simulation models of water systems is well known. Some recommendations regarding spatial and temporal requirements of rainfall input for such models can be found in the literature. Schilling (1991) proposed a temporal resolution of 1–5 minutes and a spatial resolution of 1 km for sewer modelling. Berne *et al.* (2004) suggested a temporal resolution of 5 minutes and a spatial resolution of 3 km. Jacquet *et al.* (2002) proposed a spatial resolution of 2 km. A very dense raingauge observation network would meet such requirements, but such network is impracticable because of its difficulty in installation and maintenance (Wilson & Brandes 1979).

Weather radars are increasingly being used as an alternative because of their capability of providing continuous spatial measurements and capability of detecting rainfall events to a hundred kilometers from the radar site (Wilson & Brandes 1979; Einfalt *et al.* 2004; Goudenhoofdt & Delobbe

doi: 10.2166/hydro.2012.120

2009). However, use of weather radars has been more for qualitative measurement than for quantitative estimation of the rainfall field (Uijlenhoet 2001; Sempere-Torres *et al.* 2000). The quantitative radar based rainfall estimates indeed may have large uncertainties because radars do not measure rainfall directly (Einfalt *et al.* 2004). A radar measures the back scattered energy from precipitation particles, the reflectivity. The reflectivity factor 'Z' must be converted to a rain rate 'R'. Uijlenhoet (2001) provides a detailed insight on the relationship between Z and R, and on the uncertainty in the estimation of R from Z. This uncertainty should be minimized before using radar data as input to water system simulation models by using suitable adjustment techniques (Wilson & Brandes 1979).

Mostly three types of weather radars are used in hydrometeorology: S-band, C-band and X-band radars (Collier 1989). The difference lies in the wavelength of the emitted electromagnetic waves. The S-band radars have the longest wavelength while the X-band radars have the shortest. Using a larger wavelength for radar measurement would certainly enhance the usable range but problems arise from radar beam interaction with the ground. The shorter wave length radars, although having fine spatial resolution, suffer from attenuation significantly (Einfalt *et al.* 2004). Attenuation can be caused by adsorption and scattering of cloud droplets, atmospheric gases and precipitation (Delobbe & Holleman 2006). Attenuation of radar signal increases with frequency. Due to this, the rainfall estimates from shorter wavelength radars especially those from X-band radar have to be applied very carefully. For shorter wavelength radars, rain storms close to the radar site are better sampled. Storms far from the radar sites will be sampled poorly. Hence, algorithms need to be developed by taking the attenuation effect into account. Recent algorithms are mainly based on the path integrated attenuation (PIA) at a given range. Berne & Uijlenhoet (2005) present a stochastic model to quantify the effects of attenuation on radar estimates. Vulpiani *et al.* (2006) also present algorithms to correct attenuation on C-band polarimetric weather radars. Anagnostou *et al.* (2006) corrected attenuation on the reflectivity readings from X-band dual polarization Doppler radars using a similar approach. Also, radar estimates can be affected by ground clutter. Hazenberg *et al.* (2011) observed largest improvement on the radar estimates by correcting ground clutter. The conversion of Z to R is also a crucial issue. Different Z–R conversion relationships for different rainfall types (stratiform and convective) have been observed by many researchers (e.g. Sempere-Torres *et al.* 2000). For extreme events, the uncertainty in radar measurements increases (Einfalt *et al.* 2004). Hence, special attention should be given on such events owing to the microphysical structure of raindrop size. Uijlenhoet *et al.* (2003) provide detailed insight on the variability of Z–R relationship in extreme rainfall. The vertical profile of reflectivity (VPR) should also be considered especially in the winter half year. Berne *et al.* (2005) observed a clear VPR gradient on a typical stratiform event but not in a typical convective summer thunderstorm event. It is clear that if one wants to get most optimal quality of rainfall information derived from radars, corrections have to be applied for the above-mentioned sources of errors.

The total error in point rainfall estimates obtained from radar data can be derived from raingauge data. Raingauges indeed typically provide more accurate point-wise ground measurements of rainfall (Einfalt *et al.* 2004). A network of raingauges, however, lacks spatial representation (Goudenhoofdt & Delobbe 2009) while radar can provide continuous spatial measurements over a large region (Wilson & Brandes 1979; Einfalt *et al.* 2004). Hence, merging of both forms of rainfall estimates (raingauge and radar) is advised (Creutin *et al.* 1997). Several methods exist to merge radar and raingauge data: from simple merging methods to sophisticated spatial methods. Many rigorous studies have been carried out on the evaluation of these merging methods (e.g. Delobbe *et al.* 2008; Goudenhoofdt & Delobbe 2009; Shrestha *et al.* 2010). They concluded that raw radar data can greatly be enhanced. However, radar-gauge residuals, even after radar adjustment may remain significant (Borga 2002).

It became clear from the above discussion that radar based rainfall estimates have both an advantage and a disadvantage when used as input for hydrological modelling. The advantage is the spatial information it provides on the rainfall field; the disadvantage is the uncertainty in the quantitative rainfall estimation. Several authors have shown that the advantage may prevail for specific hydrological modelling applications of specific catchments (Borga 2002; Quirmbach & Schultz 2002; Berne *et al.* 2005;

Segond *et al.* 2007). Other authors state that the usefulness of radar estimates in such applications is still under debate (Tetzlaff & Uhlenbrook 2005). Whereas radar technology offers enormous opportunity for hydrologists, there are indeed examples of good practice and failures (Einfalt *et al.* 2004). More research is required to investigate and improve both the quantitative and qualitative aspects of radar estimates. Where traditionally C- and S-band radar based rainfall estimates have been tested in catchment hydrological applications, little research has been done in testing the usefulness of X-band radar data (Thorndahl & Rasmussen 2012). X-band radars, also called Local Area Weather Radars (LAWRs), are very promising in providing local (high resolution) rainfall estimates (Willems *et al.* 2012). Such high resolution estimates are important for applications of urban hydrology or small river catchments. The hydrological application of radar estimates also depends on the type of hydrological model used. Fully distributed models are expected to synchronize better with radar based spatial rainfall inputs. Also, basin characteristics play a role. Experiences have shown that more rural (less urbanized) catchments tend to filter out the effect of the spatial rainfall variability. The direct benefit of using radar based spatial rainfall input thus is less evident for this type of catchment (Sanchez-Diezma *et al.* 2001; Segond *et al.* 2007).

Our present study contributes to this research and investigates the accuracy of radar estimates from two radars in Belgium; the C-band weather radar of the Royal Meteorological Institute of Belgium (RMI) at Wideumont and the X-band LAWR of Aquafin at Leuven. After calibration, the radar estimates are subjected to different merging procedures. The adjusted radar estimates are then applied to a lumped conceptual rainfall-runoff model for a nearby small Belgian river catchment, to investigate the usefulness of the radar based rainfall estimates in comparison with the use of raingauge data only. A brief description of the study catchment and the location of the two radars are given under 'Study area'. The 'Study area' section also provides details on the radars including the radar calibration methods applied, and on the available raingauges. The methods tested in this study for merging the raingauge and radar data and for the rainfall-runoff impact analysis are outlined under 'Methods'. Results of the application of the merging techniques and runoff impact modelling are shown and discussed under 'Results and discussion'. Final conclusions are formulated under 'Conclusions'.

STUDY AREA

Study catchment

The study catchment is located in the Flemish region of Belgium. It is the catchment of the Molenbeek tributary river of the river Dijle, which eventually flows to the river Scheldt. The catchment is situated south-east of the LAWR at Leuven and north-west of the RMI radar at Wideumont. The distances from the centroid of the catchment to the LAWR and RMI radars are approximately 5 and 125 km, respectively (Figure 1). The Molenbeek catchment is relatively flat, primarily composed of sandy soils (70%) with high hydraulic conductivity, and hence rainfall is intensively drained. The elevation ranges from 22 to 117 m above mean sea level, with a mean elevation of 59 m. About 53% of the area is used for agricultural activities, 33% of the area has a mixed type of forest, 13% of the area is urbanised and less than 1% consists of water bodies. The mean annual precipitation depth is about 800 mm, almost evenly distributed throughout the winter and summer months. The average daily temperature ranges from 4 degrees centigrade in winter to 22 degrees centigrade in summer.

Raingauges

Comparing radar estimates essentially requires ground truth data which are assumed to be correctly represented by a raingauge network. For our purpose, a network of 12 raingauges is used; four of them being operated by Aquafin, five by the Flemish Environment Agency (VMM) and the other three by the RMI of Belgium (Figure 1). The Aquafin raingauges are tipping bucket raingauges (TBRs) having a gauge resolution of 0.2 mm and a time resolution of 2 minutes. The VMM raingauges are also TBRs having a gauge resolution of 0.2 mm and a time resolution of 10 minutes. The RMI maintains quite a dense network of non-recording raingauges giving daily precipitation accumulations between 8 a.m. and 8 a.m. local time. The Aquafin and VMM raingauges were subjected to full dynamic calibration. The

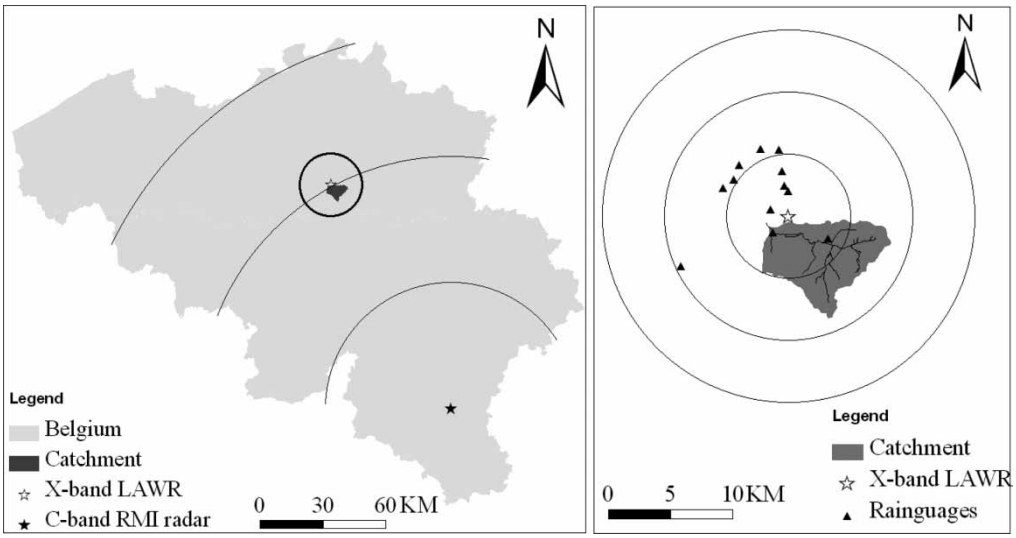

Figure 1 | Left: The study area with Belgium (grey area), the catchment (black area), the X-band LAWR (grey star) and the C-band RMI radar (black star). Thick circle indicates 15 km distance to the LAWR and thin arcs indicate the distance to the C-band RMI radar, with increments of 60 km. Right: The catchment (black area) with the location of 12 raingauges (black triangles), the LAWR (grey star) and stream network. Circles indicate the distance to the LAWR, with increments of 5 km.

calibration is performed in the field. Local wind shelter influences on these TBRs were also investigated. More information regarding this calibration and wind influences can be found in Goormans & Willems (2008).

C-band radar

The radar of RMI at Wideumont is a single-polarization C-band radar. The radar performs a volume scan every 5 minutes with reflectivity measurements up to 240 km. A Doppler scan with radial velocity measurements up to 240 km is performed every 15 min (RMI 2009). A time domain Doppler filtering is applied to remove the ground clutter. It is then subjected to an additional treatment to eliminate the residual permanent ground clutter caused by the surrounding hills. The effect of ground clutter is treated by replacing the reflectivity values collected at higher elevation (Delobbe *et al.* 2006). An advection correction procedure is applied to correct the time sampling interval effect in the accumulated maps (Delobbe *et al.* 2006). No attenuation or VPR corrections are applied. Such corrections may, however, significantly affect the rainfall estimates as is shown by Hazenberg *et al.* (2008) and Creutin *et al.* (1997). The 5 minute radar data are summed up to produce 1 h and 24 h precipitation accumulation products. The 1h product is used in this study. The radar is equipped with a linear receiver and the Z values are converted to R, based on the well-known Z–R relationship of Marshall and Palmer (Marshall *et al.* 1955), which is of the form: $Z = aR^b$. The values of a and b are chosen to be 200 and 1.6, respectively, as used by many researchers (e.g. Berne *et al.* 2005; Delobbe *et al.* 2006; Delobbe *et al.* 2008; Hazenberg *et al.* 2008; Goudenhoofdt & Delobbe 2009).

X-band radar

The X-band LAWR is installed in the densely populated city centre of Leuven, Belgium, by the Flemish Water Company Aquafin. Based on rigorous clutter tests, the LAWR is installed on the roof of the Provinciehuis building – the main office of the Province of Flemish Brabant. This location produced acceptable amounts of clutter, mainly due to a pit wall which cuts off the lower part of the beam (Goormans *et al.* 2008). The range is 15 km and reflectivity measurements are performed with a time resolution of 1 minute. The LAWR samples 450 scanlines each rotation. The radar signal values are then subjected to attenuation correction followed by a volume correction. The volume correction is to cope with the risk of partial filling at larger range. After this, clutter removal is

achieved using a clutter map. The clutter map is a radar image taken during a dry day with clear sky, where the non-zero values are assumed to be clutter (Goormans *et al.* 2008; Goormans 2011). The amount of reflected power is expressed in terms of a dimensionless quantity called 'count'. The 'count' is rescaled to 8 bit data, thus ranging from 0 to 255. Contrary to conventional weather radars like C-band weather radars, which are equipped with a linear receiver, the LAWR has a logarithmic receiver. This suggests that the conventional transformation from reflected power to R should be linear. Different researchers suggested different relationships between 'count' and 'R'. Rollenbeck & Bendix (2006) reported that a linear relationship between 'counts' and 'R' showed most stable results. This linear relationship therefore was used in the study. The conversion factor which converts 'count' to 'R' is termed as calibration factor (CF). The CF is determined based on a simple least squares method. The calibration curve is the regression line of the rain event averaged 'count' over the considered raingauge pixel versus the rain event averaged value of 'R' recorded by the raingauge. Rain events are separated based on a threshold value for the interevent time. Five different interevent times of 30, 60, 120, 180 and 240 minutes were tested. The interevent time of 60 minute produced the most stable results (Goormans 2011). Table 2 presents the CF values for the different raingauges. Table 1 shows some basic characteristics of the RMI and LAWR radars.

Table 1 | Some characteristics of the LAWR and RMI radars

Property	C-band radar	X-band LAWR
Location	Wideumont, Belgium	Leuven, Belgium
Operational since	October 2001	July 2008
Frequency	C-band (5.64 GHz)	X-band (9410 ± 30 GHz)
Mean transmit power	250 W	25 W
Height of tower	50 m	48 m
Antenna diameter	4.2 m	0.55 m
Maximum range	240 km	15 km
Time interval precipitation products	5 min	1 min
Space resolution	600 m	125 m

Table 2 | Calibration factor (CF) for Aquafin and VMM raingauges

Operator	Raingauge location	CF [(mm/hr)/(counts/min)]
Aquafin	RWZI Kessel-Lo	0.0600
	Keulenstraat	0.1131
	Hoge Beekstraat	0.0934
VMM	Derijcklaan	0.0421
	Oudstrijderslaan	0.0615
	Eenmeilaan	0.0531
	Weggevoerdenstraat	0.1601
Average		0.0833

Data periods

Owing to the rainfall patterns in Belgium, this study distinguished two data periods namely summer and winter storm periods. Convective rainfall is encountered in most of the summer storm cases and stratiform rainfall in both summer and winter periods. RMI radar data of some interesting storm periods were considered. These periods are named week 1 to week 4 as presented in Table 3; weeks 1 and 2 belongs to the summer period and weeks 3 and 4 to the winter period. The LAWR radar data are divided into two periods as per the setting of the signal processing parameters of the LAWR as presented in Table 4. For the LAWR-gauge comparison, the summer period (period-1) considered, spans from July 2, 2008 to September 30, 2008, and the winter period (period-2) from December 1, 2008 to March 31, 2009.

Table 3 | Data periods of RMI radar

Weeks	Time span
1	July 2, 2008 to July 12, 2008
2	August 3, 2008 to August 13, 2008
3	January 17, 2009 to January 23, 2009
4	February 9, 2009 to February 17, 2009

Table 4 | Data periods of LAWR radar

Period	Data periods
1	July 2, 2008 to October 8 , 2008
2	October 9 to October 31, 2008 and December 1, 2008 to present

METHODS

Radar-gauge comparison and merging

The radar-gauge comparison and merging techniques for the X-band LAWR of Leuven is briefly described in Shrestha *et al.* (2010). The same procedure has been applied for the C-band RMI radar. Three gauge-radar merging techniques, namely Range dependent adjustment, Mean field bias correction (MFB) and Brandes spatial adjustment (BRA), are applied. Range dependent adjustment assumes adjustment factors as a function of distance from the radar site. The MFB correction (Equation (1)) assumes that the radar field can be corrected by a uniform multiplicative factor while the BRA (Equation (2)) is based on the principle of Brandes (1975). The BRA distributes correction factors from the raingauge sites to each radar grid cells based on the distance between them.

If both daily raingauge and radar accumulations are greater than 1 mm then these were considered as valid pairs. This ensures that the same data set is used for comparison. For all purposes, the average counts over nine radar pixels surrounding the raingauge location is used so as to limit the effect of wind drift which can be very significant (Lack & Fox 2007).

$$\mathrm{MFB} = \frac{\sum F_i}{N} = \frac{1}{N}\sum \frac{G_i}{R_i} \tag{1}$$

$$\mathrm{BRA} = \frac{\sum_{i=1}^{N} W_i \frac{G_i}{R_i}}{\sum_{i=1}^{N} W_i} \text{ with } W_i = e^{-\frac{d^2}{k}} \text{ and } K = (2\delta)^{-1} \tag{2}$$

where MFB = mean field bias; BRA = Brandes spatial adjustment; F_i = gauge calibrated bias; N = number of valid radar-gauge pairs; G_i, R_i = gauge and radar daily accumulated values associated with gauge I; W_i = weight applied to each F_i; d = distance between the gauge and the grid point in kilometers; k = a factor controlling the degree of smoothing, and δ = mean gauge density (number of gauges divided by total area).

In order to evaluate the improvements achieved by each adjustment procedure, comparison on some goodness-of-fit statistics is made before and after an adjustment procedure. Several of these parameters are found in the literature. However, the root mean squared error (RMSE) – Equation (3), mean absolute error (MAE) – Equation (4), relative fractional bias (RFB) – Equation (5) and Nash-Sutcliffe efficiency (NSE) – Equation (6) are used in this study. The RMSE and MAE are most common parameters used for verification studies. The RFB accounts for the bias of radar estimates to gauge value in a relative manner. The NSE is usually used to assess the predictive power of hydrological models (Nash & Sutcliffe 1970), but adapted for our case accordingly.

$$\mathrm{RMSE} = \sqrt{\frac{\sum_{i=1}^{N} (R_i - G_i)^2}{N}} \tag{3}$$

$$\mathrm{MAE} = \frac{\sum_{i=1}^{N} |(R_i - G_i)|}{N} \tag{4}$$

$$\mathrm{RFB} = \frac{R_i - G_i}{G_i} \tag{5}$$

$$\mathrm{NSE} = 1 - \frac{\sum_{i=1}^{N} (G_i - R_i)^2}{\sum_{i=1}^{N} (G_i - \overline{G})^2} \tag{6}$$

where N = number of valid radar-gauge pairs; G_i, R_i = gauge and radar daily accumulated values associated with gauge I, and $\overline{G}$ = mean of gauge readings.

Rainfall-runoff impact model

For the impact analysis of the different types of rainfall input on the stream flow downstream the Molenbeek catchment, a lumped conceptual rainfall-runoff model was set up. This was done using the generalized lumped conceptual and parsimonious model structure-identification and calibration procedure by Willems (2000, 2011). This procedure, hereafter denoted as the VHM approach according to a Dutch abbreviation (Veralgemeend conceptueel Hydrologisch Model), is a top-down approach where the lumped conceptual rainfall runoff model is set up in a transparent, step wise way (Willems 2000, 2011). It makes use of multiple and

non-commensurable information derived from river flow series by means of a number of sequential time series processing tasks. These pre-processing tasks are carried out in an MS Excel based tool called Water Engineering Time Series Processing Tool (WETSPRO) (Willems 2009). The required pre-processing tasks are as follows. (1) Transformation of the river flow series in a series of lumped rainfall-runoff discharges. (2) Separation of the rainfall-runoff series in subflow series using a numerical digital filter. The river flow series can be separated into quick flow (overland flow and interflow) and slow flow (baseflow). (3) Split of the rainfall-runoff series in individual nearly independent quick and slow flow events and peak over threshold (POT) values. The POTs can be extracted to that of quick flow events and slow flow events.

The information acquired through the pre-processing of the river flow time series is then used for step-wise model-structure identification and calibration. In this step, lumped representations of different specific rainfall-runoff process equations are identified and calibrated to related subsets of model parameters. This includes the following sub-steps: identification and calibration of the routing submodels; identification and calibration of the soil moisture storage submodel where the rain water fraction to soil moisture, the maximum soil moisture content and the threshold moisture content for evapotranspiration are identified; and identification and calibration of the submodels describing the rainfall fractions of quick (overland and interflow) and slow (base) flows.

The method aims to derive a parsimonious model structure. The model requires catchment average evapotranspiration and rainfall time series as input. This study used an hourly time step.

Further details of the VHM model can be obtained through Willems (2000, 2011) or Taye *et al.* (2010). The prior time series processing techniques are extensively discussed in Willems (2009).

Rainfall-runoff model calibration and validation

The calibration period is selected from January 1, 2006 to February 28, 2009. Validation of the calibrated parameters is made in another independent period from September 10, 2003 to December 31, 2005. In this study, the rainfall derived from the raingauge network was perceived as more robust and hence considered as reference rainfall (P_{ref}). The calibration of the model parameters is done using P_{ref} using a heuristic approach. The parameters thus derived are used to see the performance of adjusted radar estimates.

The rainfall-runoff model performance was evaluated based on the WETSPRO tool (Willems 2009). It allows the model performance evaluation to be carried out in different flow components, hydrological high and low flow extremes and flow volumes based on the assessment of graphical displays as complementary to the traditional goodness of fit statistics. We used two basic goodness-of-fit statistics, the mean squared error (MSE), Equation (7) and the Nash-Sutcliffe Efficiency (Nash & Sutcliffe 1970), Equation (8).

Evaluation of impact results

While calibrating a rainfall-runoff model, it is sometimes possible to compensate the errors induced by systematic deviation in rainfall estimates by calibrating the model parameter untill results with sufficient accuracy are obtained. Hence, we adopted a methodology whereby the model which is calibrated against P_{ref} will not be re-calibrated against the radar estimates. This approach keeps model parameters and related model parameters' uncertainty the same thus allows to evaluate the significance of the radar estimates to reproduce the stream flow. Besides P_{ref}, the adjusted radar rainfall estimates from C-band RMI radar and X-band LAWR form two alternative rainfall descriptors. Hereby, two NSE values can be defined. The NSE_{obs} (Equation (9)), can be calculated with reference to the observed discharge series to the modelled discharge produced by P_{ref}. The simulated flow driven by the reference P_{ref} is referred to as the reference flow (Q_{ref}). The difference between the reference flow and flow driven by an alternative rainfall descriptor is the relative error induced due to the tested alternative rainfall. A modified definition of Equation (9) is introduced to measure the performance of the calculated runoff (Q_{cal}) in comparison to Q_{ref}.

$$\mathrm{MSE} = \frac{\sum_{i=1}^{N} \left(Q_{m,i} - Q_{o,i}\right)^2}{N} \tag{7}$$

$$\mathrm{NSE}_{\mathrm{obs}} = 1 - \frac{\sum_{i=1}^{N} \left(Q_{m,i} - Q_{o,i}\right)^2}{\sum_{i=1}^{N} \left(Q_{o,i} - \overline{Q}_o\right)^2} \quad (8)$$

$$\mathrm{NSE}_{\mathrm{ref}} = 1 - \frac{\sum_{i=1}^{N} \left(Q_{\mathrm{cal},i} - Q_{\mathrm{ref},i}\right)^2}{\sum_{i=1}^{N} \left(Q_{\mathrm{ref},i} - \overline{Q}_{\mathrm{ref}}\right)^2} \quad (9)$$

where $\mathrm{NSE}_{\mathrm{obs}}$ and $\mathrm{NSE}_{\mathrm{ref}}$ = modified form of Nash-Sutcliffe efficiency; i = the number of observations (1, N); $Q_{m,i}$ = modelled discharge; $Q_{o,i}$ = observed discharge; $\overline{Q}_o$ = mean of observed discharge; $Q_{\mathrm{cal},i}$ = calculated discharge; $Q_{\mathrm{ref},i}$ = reference discharge; $\overline{Q}_{\mathrm{ref}}$ = mean of reference discharge.

RESULTS AND DISCUSSION

Evaluation of merging techniques on X-band LAWR

Using an average value of CF (as in Table 2) showed a significant fluctuation on the radar and gauge values for cumulative rainfall volumes of the summer period as well as the winter period. The RFB ranged from +1.25 (125% overestimation) to −0.57 (57% underestimation). It is observed that the radar tends to overestimate rainfall in pixels located close to the LAWR and tends to underestimate rainfall in pixels located away from the LAWR location (Figure 2(a)). It is therefore easy to understand that there exists some kind of range dependency on CF values and hence on the radar estimated rainfall values. Combining a second degree polynomial equation (CF = $0.0006\ r^2 + 0.015r + 0.0159$, for $r < 1.5$ km) and a power function (CF = $0.0272\ r^{0.8226}$, for $r \geq 1.5$, where r is the distance to the LAWR in km), the range dependency aspect is addressed. These equations are obtained by fitting the best curve on the calculated set of CF values. The RFB, after range dependent adjustment, shows no trend of either overestimation or underestimation as the range increases (Figure 2(b)).

After range dependency adjustments on the LAWR estimates, the radar field was subjected to MFB adjustment. The MFB for the summer and winter periods is calculated as 1.015 and 0.974, respectively, as the mean of log values of the gauge calibrated bias (F_i). The log transformation was applied because it was found that the individual F_i followed a nearly perfect log-normal distribution. No serious underestimation and overestimation of rainfall volumes on both periods is observed as indicated by the MFB values close to 1.0. Upper and lower limits for the 90%-confidence interval of the F_i have been calculated for both periods. It is observed that the real MFB adjustment factor for the summer period lies between 0.953 and 1.076. For the winter period, the MFB factor lies between 0.920 and 1.030. After MFB correction, the radar field was smoothed by applying the BRA adjustment.

The improvements on the raw LAWR estimates after each adjustment procedure have been well reflected in the

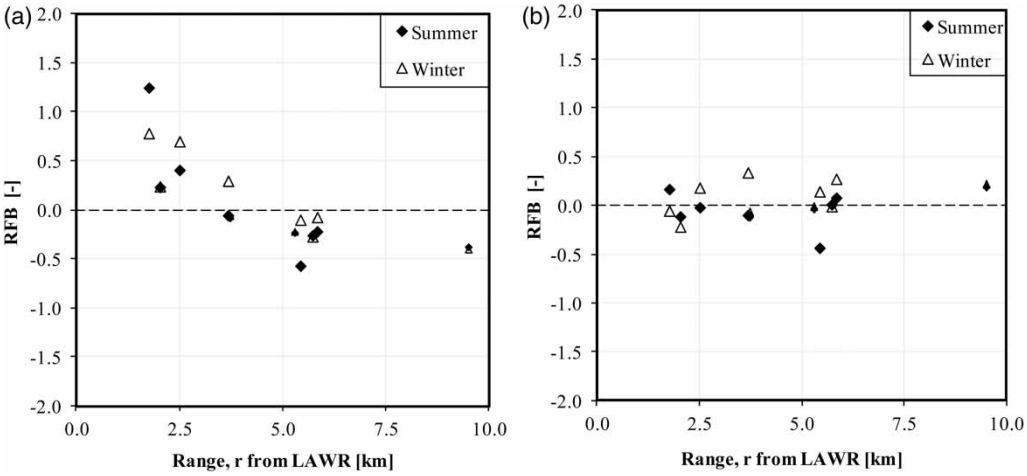

Figure 2 | Evolution of relative field bias (RFB) with range: (a) before range dependency correction and (b) after range dependency correction on the LAWR based estimates for both summer and winter periods.

calculated goodness-of-fit statistics (Figure 3(a) and 3(b)). Decreasing RMSE and MAE values (Figure 3(a)) and increasing NSE values (Figure 3(b)) are observed when the raw radar data are subjected to subsequent adjustment procedures. For both periods, the improvements are significant, but residuals are not negligible even after the adjustments. Winter periods show higher RMSE, MAE and lower NSE meaning that estimates on summer periods are slightly better. The NSE value after adjustment for the summer period is 0.7, while the same for the winter period is only 0.55 after applying adjustment procedures on raw LAWR estimates.

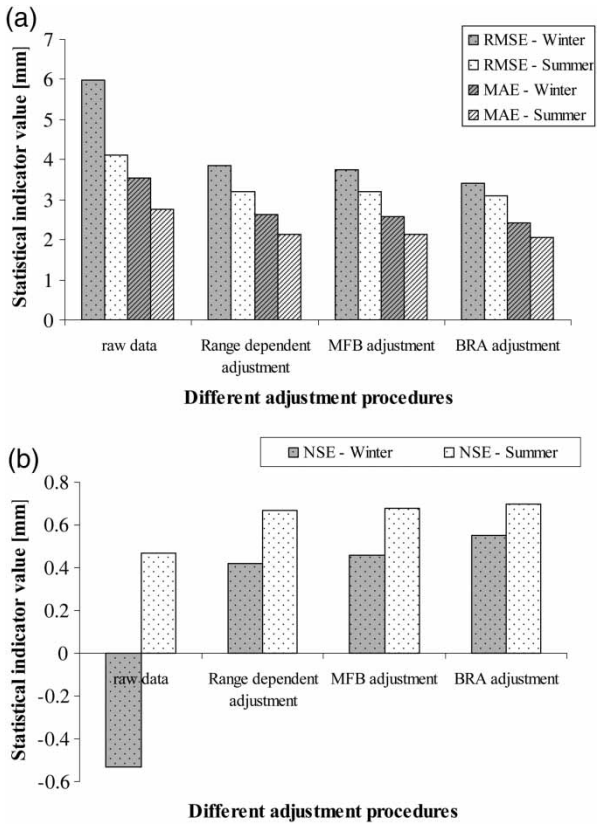

Figure 3 | Evolution of different statistical indicators with different adjustments on the LAWR based estimates: (a) the RMSE and MAE, and (b) the NSE.

Evaluation of merging techniques on C-band RMI radar

Analysis of the RFB for both summer and winter periods showed no range dependency. No systematic trend of the RFB variation with range was observed. Hence, the raw radar estimates were directly subjected to the MFB and then to the BRA adjustment. The MFB values for summer weeks and winter weeks are 0.732 and 2.217, respectively. The 90%-confidence interval was also calculated. The upper and lower confidence interval limits for summer weeks (weeks 1 and 2) are found to be 0.808 and 0.662, respectively. For winter weeks (weeks 3 and 4), the upper and lower limits are found to be 2.414 and 2.036, respectively.

The scatter plot of radar estimates before and after MFB is shown in Figure 4. Raw radar estimates tend to overall overestimate the daily accumulated rainfall values as suggested by the MFB value less than 1.0. However, the scatter plot for the summer period shows a quite complex picture. For higher rainfall values, the radar tends to

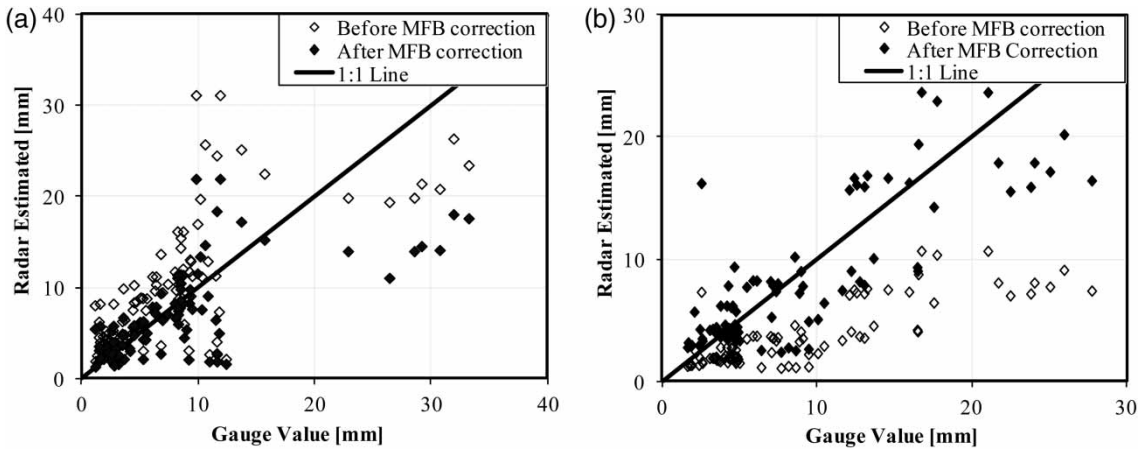

Figure 4 | Scatter plot of daily rainfall volumes before and after mean field bias correction (MFB) on RMI radar estimates (a) for summer weeks and (b) for winter weeks.

underestimate the rainfall intensities while for medium rainfall values, it is the reverse (Figure 4(a)). This complexity can be attributed to the different types of precipitation events that were observed (e.g. deep thunderstorm convection to stratiform frontal system) in the summer half year, all of these rainfall patterns having different rainfall microphysics. The applied Z–R relationship also might play a role as different Z–R relationships for different types of rainfall are evident from the literature. Better results could be obtained by analyzing the rainfall structure and applying a suitable Z–R relationship (e.g. $Z = 300R^{1.4}$ for convective storm events; Einfalt *et al.* 2004). The used Z-R relationship ($Z = 200\ R^{1.6}$) is typically suitable for startiform events (Einfalt *et al.* 2004) which tend to overestimate rainfall rate as compared to $Z = 300\ R^{1.4}$. The underestimation for higher rainfall values might be because of attenuation especially rain-induced attenuation. For the winter period, the situation is different. The radar estimates tend to seriously underestimate rainfall volumes, which is in accordance with the findings of other studies using the same type of radar data for the winter period (e.g. Hazenberg *et al.* 2011). As the entire raingauge network lies between 118 and 129 km from the radar location, the radar beam is located rather high at those locations, and might miss the raindrops, resulting in underestimation of rainfall rates. Also, Belgium experiences mostly stratiform rainfall in winter periods. The stratiform rainfall originates from stratiform clouds which are low in elevation. This also favors possible overshooting phenomena. This might also be because of VPR variation as observed by Berne *et al.* (2005) for typical startiform storms. At higher elevation, the radar signal samples snow rather than raindrops which can lead to huge underestimation of the reflected power hence the underestimation of rainfall rates. The underestimation in winter period is also reflected by a rather high MFB value of 2.217. After the MFB correction, the rainfall bias strongly reduces (Figure 4(b)).

After the MFB adjustment, the smoothed radar field was subjected to the BRA adjustment. Subsequent improvement on the radar estimates are clearly reflected in the goodness-of-fit statistics. Significant improvements are observed in the winter weeks. The initial NSE of −0.10 is improved to 0.66 after the adjustments in the winter weeks (Figure 5(b)). In terms of the RMSE, the summer weeks showed higher value of 4.90 mm compared to 3.76 mm of the winter weeks. The MAE, however, does not show the same trend. The MAE is lower in summer weeks (3.02 mm) than in winter weeks (4.38 mm) (Figure 5(a)).

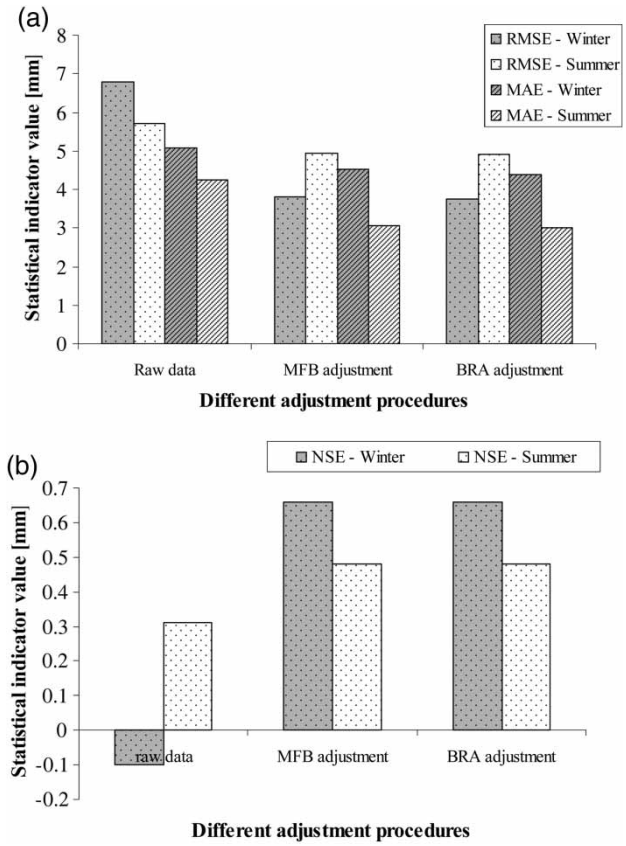

Figure 5 | Evolution of different statistical indicators with different adjustments on the RMI radar based estimates: (a) the RMSE and MAE, and (b) the NSE.

Comparison of C and X-band estimates

Table 5 shows different statistical indicators for the summer and winter periods after the adjustment procedures are applied on the LAWR and RMI estimates. As the statistical

Table 5 | Different statistical indicators for the summer and winter periods after the adjustments on the LAWR and RMI radar based estimates

Statistical indicators	Summer period/weeks		Winter period/weeks	
	LAWR	RMI	LAWR	RMI
RMSE [mm]	3.09	4.91	3.40	3.76
MAE [mm]	2.06	3.02	2.42	4.38
NSE [–]	0.70	0.48	0.55	0.66

parameters indicate, the LAWR local rainfall estimates are better than the RMI estimates. The RMSE and MAE values are lower and the NSE values are higher for the adjusted LAWR estimates than the adjusted RMI estimates. Better performance of the LAWR estimates could be attributed to its high resolution (125×125 m) compared with the RMI (600×600 m). After adjustment, the LAWR estimates tend to represent the summer period better than the winter period, while the RMI estimates tend to represent the winter weeks better than the summer weeks.

Table 6 shows the cumulative rainfall volumes for the weeks 1 to 4 recorded by the three rainfall descriptors: P_{ref}, adjusted LAWR and adjusted RMI estimates. A deviation index is also calculated based on the absolute relative difference of radar estimates to the P_{ref}, normalized by the P_{ref} and expressed as percentage. As it can be seen, the deviation index is higher for RMI radar based estimates for summer weeks (weeks 1 and 2) than for LAWR estimates. For winter weeks (week 3 and 4), the situation is in the reverse.

Table 6 | Cumulative rainfall volumes for the weeks 1 to 4 estimated from different rainfall descriptors

	Rainfall (mm)			Deviation index (%)	
Weeks	P_{ref}	LAWR	RMI	LAWR	RMI
1	49.72	45.68	55.79	8.1	12.2
2	67.02	58.26	43.98	13.1	34.4
3	44.40	41.26	45.09	7.1	1.6
4	49.05	28.36	47.94	42.2	2.3

Figure 6 shows accumulated rainfall volume estimated from the adjusted RMI radar and adjusted LAWR data over the catchment for a storm belonging to week 2. This storm spans for 8 hours (2008–08–03 19:00 to 2008–08–04 2:00) for which the weighted-average rainfall recorded by the rain-gauge network is 30.7mm. The catchment average rainfall estimated from the RMI radar is 17.4 mm while the LAWR estimated rainfall is 20.11 mm. The pixel to pixel variation of the accumulated rainfall recorded by the RMI radar is from 11.3 mm to 27.6 mm. For the LAWR, the variation is from 0 mm to 29.7 mm, some pixels do not record even a single millimeter of rainfall. For such an intense summer event, the variation observed in the RMI estimates might be justified but the variation observed in the LAWR estimates is debatable. In the south-west window of the LAWR radar sector, some patches are observed with even zero rainfall values. This seems quite unnatural. The LAWR is installed on the roof of the provinciehuis building of 48m above the ground level. The presence of a pit wall in this location acts like a clutter fence which cuts the lower part of the radar beam. This should result in a decrease in ground clutter (Goormans *et al.* 2008). This is ideal since X-band radars have large vertical opening angle and are more susceptible to direct ground clutter even at small ranges. The clutter map observed in a day with clear sky shows minimal clutter in comparison to other tested

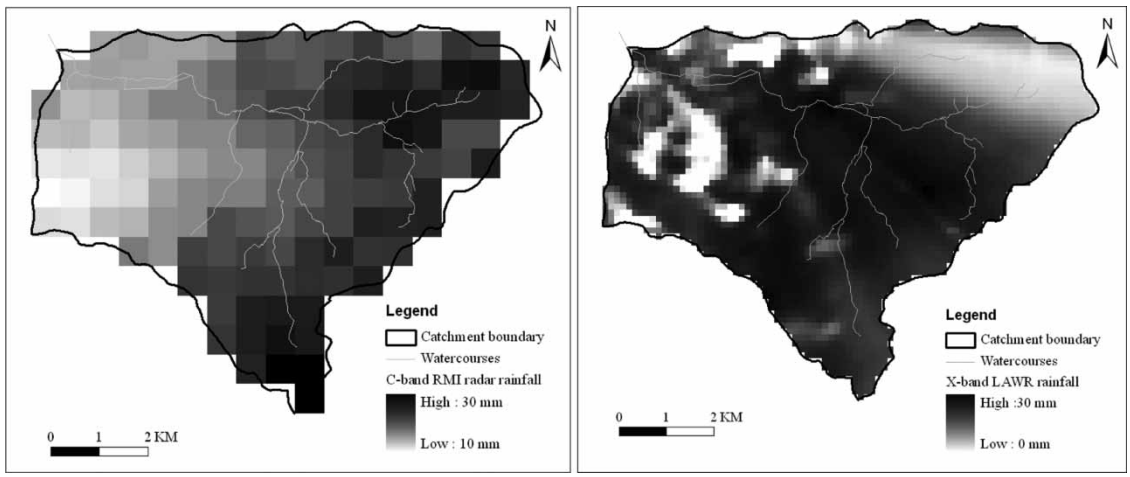

Figure 6 | Accumulated rainfall volume for a storm event of week 2 (duration of 8 hours, from 2008–08–03 19:00 to 2008–08–04 2:00) recorded by the RMI radar (left) and the LAWR (right) after adjustment procedures.

sites (four sites were tested, details on Goormans *et al.* 2008) but some patches of strong clutter are observed in short distances and in a south-west direction (Goormans *et al.* 2008). The resulting reflectivity values on those patches would result in zero or near zero reflectivity values while subtracting the clutter map. This issue either requires special ground clutter adjustment algorithms or more advanced radar-gauge merging techniques. In this study, we limit ourselves to the above-mentioned radar-gauge merging techniques; see under 'Radar-gauge comparison and merging'.

Rainfall-runoff model calibration

Table 7 shows the calibrated VHM rainfall-runoff model parameters for the Molenbeek case.

Table 8 and Figures 7 and 8 show the results of the model performance evaluation. The goodness-of-fit statistics and graphical plots show clearly the robustness of model calibration for the different flow components and extreme conditions. The MSE values for the peak quick and slow flow periods are found to be 1.06 and 1.01 $m^3 s^{-1}$, respectively while the NSE values for these flows are found to be 0.90 and 0.92, respectively.

Table 7 | Calibrated VHM parameters with a short description

Storage sub-model parameters		
U_{max} (Maximum soil water content)	500	mm
U_{evap} (Soil water constant for maximum evapotranspiration)	200	mm
Overland flow model		
$a_{OF,1}$ (Surface runoff separation process parameter)	0.052	–
$a_{OF,2}$ (Surface runoff separation process parameter)	1.5	–
$a_{OF,3}$ (Surface runoff separation process parameter)	0.3	–
Inter flow model		
$a_{IF,1}$ (Interflow separation process parameter)	0.015	–
$a_{IF,2}$ (Interflow separation process parameter)	2.5	–
$a_{IF,3}$ (Interflow separation process parameter)	0	–
Flow routing parameters		
K_{BF} (Time constant for routing baseflow)	3,500	hr
K_{IF} (Time constant for routing interflow)	50	hr
K_{OF} (Time constant for routing overland flow)	5	hr

Table 8 | Some goodness-of-fit statistics on the VHM model peak flow results

Flow periods	Number of POTs	MSE [m^3/s]	NSE [–]
Quick flow periods	273	1.06	0.90
Slow flow periods	13	1.01	0.92

Figure 7 shows modelled versus observed peak and low flows. As can be seen, the model shows almost no bias (overlapping of the mean deviation line and the bisector line) but shows some scatter.

Figure 8 shows empirical extreme value distributions for peak and low flows. As can be seen, the peak flow quantiles tend to grow with increasing return period in a similar fashion as the observed data but are underestimated for higher return periods. For low flows, the model tends to overestimate the flows for lower return periods but tends to underestimate the low flows for higher return periods.

Rainfall-runoff model impact results

Figure 9 shows simulated river discharges from different rainfall descriptors: P_{ref}, LAWR and RMI for the weeks 1 to 4. For the summer weeks (weeks 1 and 2), the LAWR derived stream flows better match the observed flows than the RMI derived flows. The RMI derived flows show lower peaks especially for week 2. For the winter periods, the LAWR derived flows tend to underestimate the peak flows while the RMI derived flows tend to overestimate the peaks.

Figure 10 shows the NSE_{ref} values for the LAWR and the RMI radar based flows for the weeks 1 to 4. The NSE_{ref} values vary from 0.58 to 0.90 for the LAWR and 0.44 to 0.82 for the RMI. On average, the NSE_{ref} value for the LAWR based flow is 0.73, while it is 0.63 for the RMI based flow. The NSE_{ref} value close to 1.0 means the alternative rainfall descriptor can reproduce the flows with same accuracy as P_{ref}. In that respect, the LAWR estimates are better than the RMI estimates. On average, the summer weeks (weeks 1 and 2) showed lower NSE_{ref} value than the winter weeks (week 3 and 4) for both radar estimates. For the winter weeks, the NSE_{ref} values are as high as 0.90, which indicates that there is no significant difference in using raingauge derived rainfall estimates in comparison with the radar based high resolution

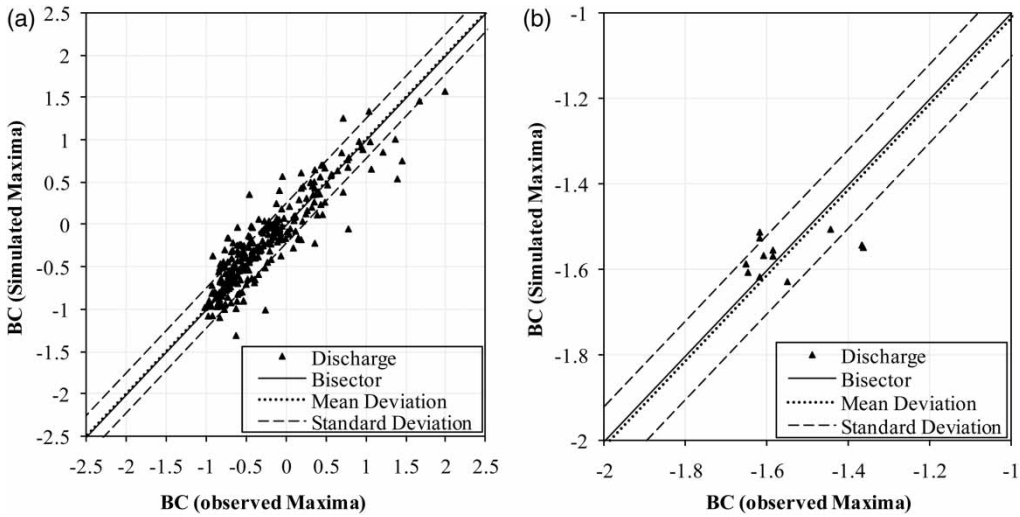

Figure 7 | Graphical comparison of nearly independent (a) peak flow maxima and (b) slow flow minima.

rainfall information. This is at least true for Belgium where winter storms typically have low intensity and low spatial variability and the raingauge network can represent this low variability with some accuracy. For the summer weeks, the low NSE_{ref} values indicate that the simulation capability is different for the raingauge derived rainfall field versus the radar estimated rainfall field. Hence it can be an opportunity for hydrologists to increase the predictive capability of models by using radar estimated rainfall field data. At the same time, the rainfall micro-physics in the summer half year can vary significantly as different types of precipitation from thunderstorm convection to stratiform frontal events can be observed for that season. To obtain better results, each storm needs to be analyzed separately. The low NSE_{ref} values for the summer weeks could also be attributed to non-optimal radar-gauge merging techniques which need further investigation.

CONCLUSIONS

The paper evaluated the accuracy of C- and X-band radar estimates. The adjusted radar estimates were used as input in a

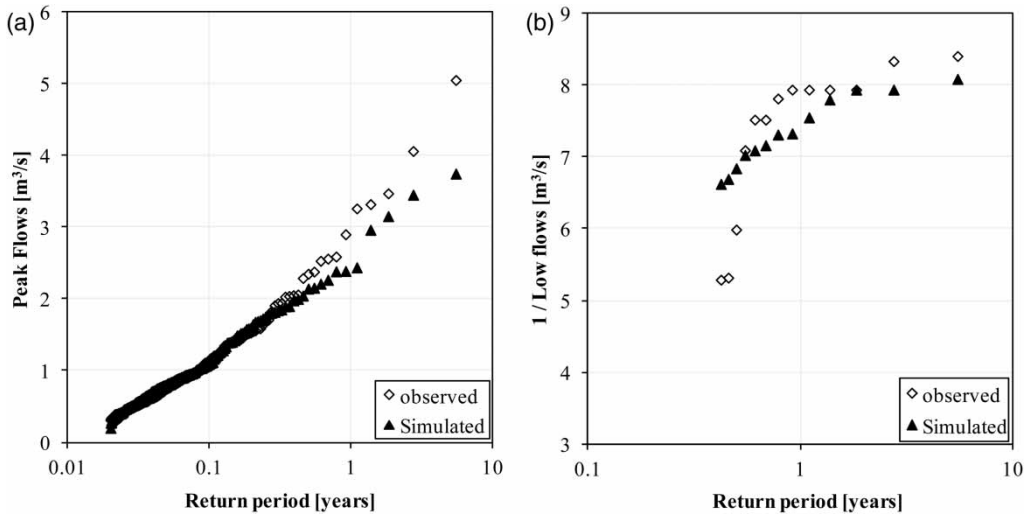

Figure 8 | Graphical comparison of (a) peak flow empirical extreme value distributions and (b) low flow empirical extreme value distributions.

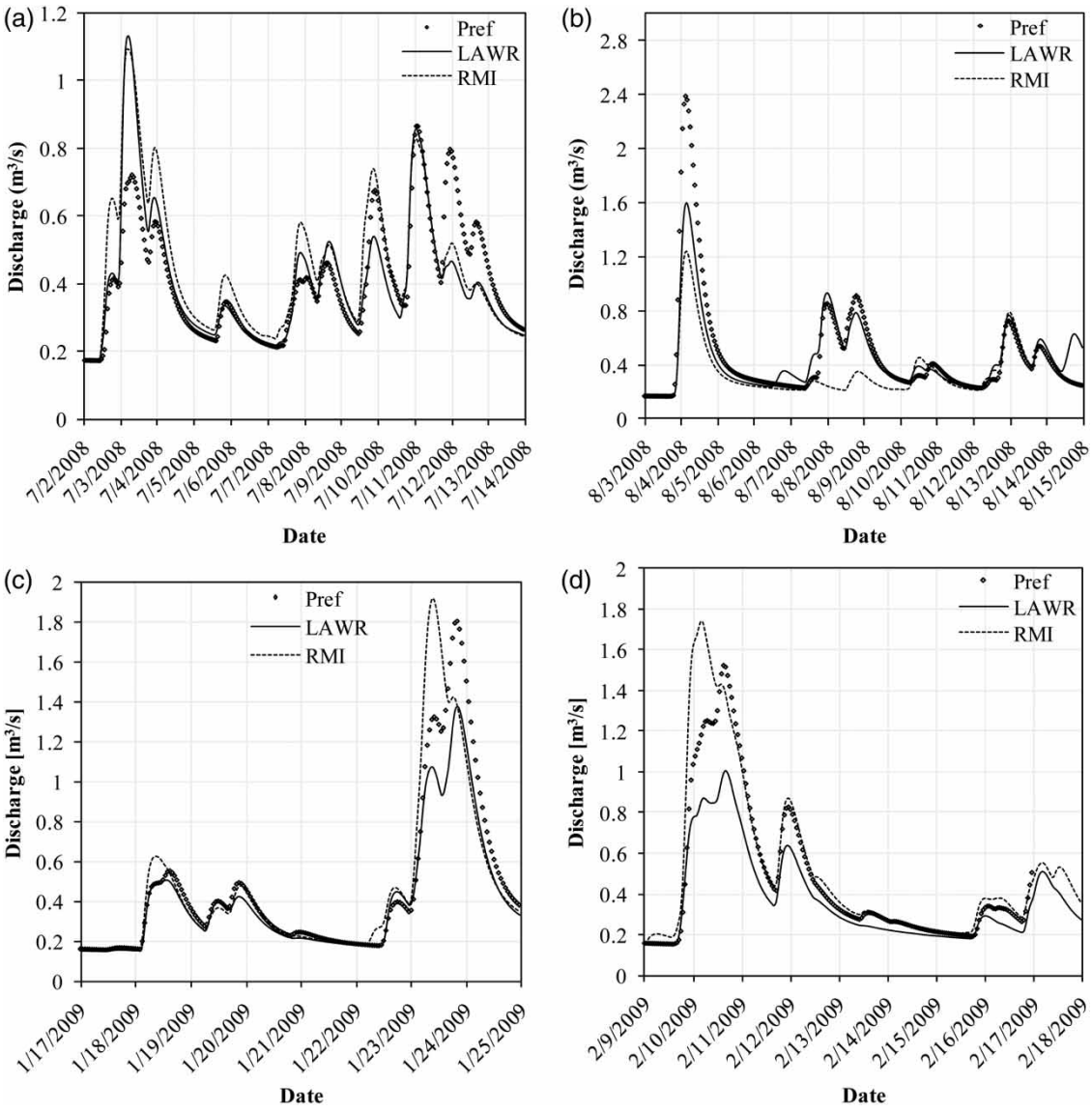

Figure 9 | Simulated stream flows for (a) week 1, (b) week 2, (c) week 3 and (d) week 4 derived by three rainfall descriptors: Pref – reference rainfall, LAWR – adjusted estimates from the X-band LAWR and RMI – adjusted estimated form the C-band RMI radar.

lumped conceptual model to simulate stream flow. The main conclusions that can be drawn from the study are as follows. Raw radar estimates need to be adjusted using suitable radar-gauge merging techniques before being used as input in any model especially if the raw radar reflectivity values are not corrected for multiple sources of errors (ground clutter, advection, attenuation, vertical profile of reflectivity, etc).

The simple gauge-radar merging techniques such as range dependency adjustment, mean field bias correction and Brandes spatial adjustment can improve the radar estimates to a great extent.

The adjusted radar estimates of the X-band local area weather radar were found to be more accurate than estimates of the C-band radar.

In terms of stream flow simulation, the predictive capabilities of adjusted radar estimates did not show much difference compared to raingauges for the winter weeks. This was, however, different for the summer weeks.

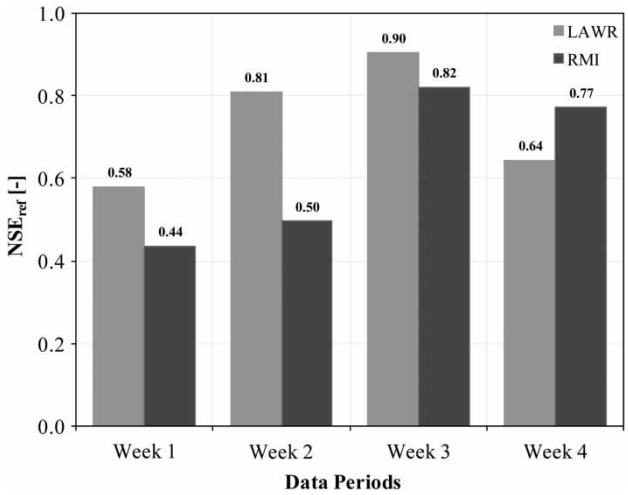

Figure 10 | NSE_{ref} values for the LAWR and RMI estimates for weeks 1 to 4.

Significant differences in stream flow simulation results were obtained for that season signifying the complex rainfall structure in the summer half year in comparison with the winter half year.

This study is carried out using data from a relatively short period, which is one of the limitations of the study. Also, the rainfall microphysical structures are not analyzed in the study. This is important especially for the summer half year. For the RMI radar, the possibility of different Z–R relationship on different periods is not analyzed. For the LAWR, the issue of optimal CF values is still there. The use of a fully distributed model instead of a lumped hydrological model and impact investigation for a more urbanized catchment are recommended issues for further investigation in the analysis of the basin response.

ACKNOWLEDGEMENTS

N. K. Shrestha received a scholarship from the Flemish Interuniversity Council – University Development Cooperation (VLIR-UOS) to pursue a Masters degree in Water Resources Engineering under the Interuniversity Program in Water Resource Engineering (IUPWARE) organized by KU Leuven and Free University of Brussels (VUB). The authors would like to thank Aquafin, VMM and RMI for providing the data used in this study. The authors appreciate the technical support of Mr Laurent Delobbe and Mr Edouard Goudenhoofdt of RMI.

REFERENCES

Anagnostou, E. N., Grecu, M. & Anagnostou, M. N. 2006 X-band polarimetric radar rainfall measurements in keys area microphysics project. *J. Atmos. Sci.* **63**, 187–203.

Berne, A. & Uijlenhoet, R. 2005 A stochastic model of range profiles of raindrop size distributions: Application to radar attenuation correction. *Geophys. Res. Lett.* L10803.

Berne, A., Delrieu, G., Creutin, J.-D. & Obled, C. 2004 Temporal and spatial resolution of rainfall measurements required for urban hydrology *J. Hydrol.* **299**, 166–179.

Berne, A., Heggeler, M., Uijlenhoet, R., Delobbe, L., Dierickx, Ph. & de Wit, M. 2005 A preliminary investigation of radar rainfall estimation in the Ardennes region and a first hydrological application for the Ourthe catchment. *Nat. Hazards Earth Syst. Sci.* **5**, 267–274.

Borga, M. 2002 Accuracy of radar rainfall estimates for streamflow simulation. *J. Hydrol.* **267**, 26–39.

Brandes, E. A. 1975 Optimizing rainfall estimates with the aid of radar. *J. Appl. Meteor.* **14**, 1339–1345.

Collier, C. G. 1989 *Applications of Weather Radar Systems – A Guide to Uses of Radar Data in Meteorology and Hydrology*. Ellis Horwood Limited, Chichester.

Creutin, J.-D., Andrieu, H. & Faure, D. 1997 Use of a weather radar for the hydrology of a mountainous area. Part II: radar measurement validation. *J. Hydrol.* **193**, 26–44.

Delobbe, L., Dehem, D., Dierickx, P., Roulin, E., Thunus, M. & Tricot, C. 2006 Combined use of radar and gauge observations for Hydrological applications in the Walloon Region of Belgium. In *4th Eur. Conf. on Radar in Meteorology and Hydrology (ERAD 2006)*, Barcelona, Spain, 18–22 September 2006.

Delobbe, L., Bastin, G., Dierickx, P., Goudenhoofdt, E., Leclercq, G., Moens, L. & Thunus, M. 2008 Evaluation of several radar-gauge merging techniques for operational use in the Walloon region of Belgium. Int. Symp. on Weather Radar and Hydrology, Grenoble, France, 10–12 March 2008.

Delobbe, L. & Holleman, I. 2006 Uncertainties in radar echo top heights used for hail detection. *Meteorol. Appl.* **13**, 361–374.

Einfalt, T., Arnbjerg-Nielsen, K., Golz, C., Jensen, N. E., Quirmbach, M., Vaes, G. & Vieux, B. 2004 Towards a roadmap for use of radar rainfall data in urban drainage. *J. Hydrol.* **299**, 186–202.

Goormans, T. 2011 Analysis of local weather radar data in support of sewer system modelling. PhD thesis, Katholieke Universiteit Leuven, Faculty of Engineering, Leuven, Belgium.

Goormans, T. & Willems, P. 2008 Correcting rain gauge measurements for calibration of an X-band weather radar. In *11th Int. Conf. on Urban Drainage*, Edinburgh, UK, 31 August–5 September 2008.

Goormans, T., Willems, P. & Jensen, N. E. 2008 Empirical assessment of possible X-band radar installation sites, based on on-site clutter tests. In *5th Eur. Conf. on Radar in Meteorology and Hydrology (ERAD 2008)*, Helsinki, Finland, 30 June–4 July 2008.

Goudenhoofdt, E. & Delobbe, L. 2009 Evaluation of radar-gauge merging methods for quantitative precipitation estimates. *Hydrol. Earth Syst. Sci.* **13**, 195–203.

Hazenberg, P., Leijnse, H. & Uijlenhoet, R. 2011 Radar rainfall estimation of stratiform winter precipitation in the Belgian Ardennes. *Water Resour. Res.* **47**.

Hazenberg, P., Leijnse, H., Uijlenhoet, R. & Delobbe, L. 2008 Hydrological modeling of the Ourthe catchment using both radar and raingauge data. In *Proceedings of the Int. Sym. on Weather Radar and Hydrology*, 10–15 March 2008, Grenoble, France.

Jacquet, G., Piatyszek, E. & Lyard, S. 2002 Radar-based rainfall input requirements: synthesis of US and French 10 years experience. In: *Proc. 9th Int. Conf. on Urban Drainage* (E. W. Strecker & W. C. Huber, eds). Portland, Oregon, USA.

Lack, S. A. & Fox, N. I. 2007 An examination of the effect of wind drift on radar-derived surface rainfall estimations. *Atmos. Res.* **85**, 217–229.

Marshall, J. S., Hitschfeld, W. & Palmer, W. M. 1955 Advances in radar weather. *Adv. Geophys.* **2**, 1–56.

Nash, J. E. & Sutcliffe, J. V. 1970 River flow forecasting through conceptual models part I – a discussion of principles. *J. Hydrol.* **10**, 282–290.

Quirmbach, M. & Schultz, G. A. 2002 Comparison of raingauge and radar data as input to an urban rainfall-runoff model. *Wat. Sci. Tech.* **45** (2), 27–33.

RMI 2009 Koninklijk Meteorologisch Instituut, in English: Royal Metrological Institute. Website: http://www.meteo.be/meteo/view/.

Rollenbeck, R. & Bendix, J. 2006 Experimental calibration of a cost-effective X-band weather radar for climate ecological studies in southern Ecuador. *Atmos. Res.* **79**, 296–316.

Sanchez-Diezma, R., Sempere Torres, D., Creutin, J. D., Zawadzki, I. & Delrieu, G. 2001 Factors affecting the precision of radar measurement of rain. An assessement from an hydrological perspective. In *Proc. of the 30th Int. Conf. on radar meteorology*, American Meteorological Society, Munich, pp. 573–575.

Schilling, W. 1991 Rainfall data for urban hydrology: what do we need? *Atm. Res.* **27**, 5–21.

Segond, M. L., Wheater, H. S. & Onof, C. 2007 The significance of spatial rainfall representation for flood runoff estimation. A numerical evaluation based on the Lee catchment. *UK. J. Hydrol.* **347**, 116–131.

Sempere-Torres, D., Sanchez-Diezma, R., Zawadzki, I. & Creutin, J.D. 2000 Identification of stratiform and convective areas using radar data with application to the improvement of DSD analysis and Z-R relations. *Phys. Chem. Earth* **25**, 895–990.

Shrestha, N. K., Goormans, T. & Willems, P. 2010 Accuracy of X-band Local Area Weather Radar (LAWR) of Leuven and its First Hydrological Application for River Catchment Modelling. In: *9th Int. Conf. on Hydroinformatics 2010* (J. Tao, Q. Chen & S.-Y. Liong, eds). 7–11th September 2010, China. Chemical Industry Press, Tianjin, pp. 1647–1654.

Taye, M. T., Ntegeka, V., Ogiramoi, N. P. & Willems, P. 2010 Assessment of climate change impact on hydrological extremes in two source regions of the Nile River Basin. *Hydrol. Earth Syst. Sci* **7**, 5441–5465.

Tetzlaff, D. & Uhlenbrook, U. 2005 Effects of spatial variability of precipitation for process-oriented hydrological modelling: results from two nested catchments. *Hydrol. Earth Syst. Sci.* **9**, 29–41.

Thorndahl, S. & Rasmussen, M. R. 2012 Marine X-band weather radar data calibration. *Atmos. Res.* **103**, 33–44.

Uijlenhoet, R. 2001 Raindrop size distributions and radar reflectivity–rain rate relationships for radar hydrology. *Hydrol. Earth Syst. Sci.* **5**, 615–627.

Uijlenhoet, R., Smith, J. A. & Steiner, M. 2003 The microphysics of extreme rainfall rates. *J. Atmos. Sci.* **60**, 1220–1238.

Vaes, G., Willems, P. & Berlamont, J. 2005 Areal rainfall correction coefficients for small urban catchments. *Atmos. Res.* **77**, 48–59.

Velasco-Forero, C. A., Sempere-Torres, D., Cassiraga, E. D. & Gómez-Hernández, J. J. 2008 A non-parametric automatic blending methodology to estimate rainfall fields from rain gauge & radar data. *Adv. Water Res.* **32**, 986–1002.

Vulpiani, G., Marzano, F. S., Chandrasekar, V., Berne, A. & Uijlenhoet, R. 2006 Rainfall rate retrieval in presence of path attenuation using C-band polarimetric weather radars. *Nat. Hazards Earth Syst. Sci.* **6**, 439–450.

Willems, P. 2000 Probabilistic immission modelling of receiving surface waters. PhD thesis, Katholieke Universiteit Leuven, Faculty of Engineering, Leuven, Belgium.

Willems, P. 2001 Stochastic description of the rainfall input errors in lumped hydrological models. *Stoch. Env. Res. Risk Assess.* **15**, 132–152.

Willems, P. 2009 A time series tool to support the multi-criteria performance evaluation of rainfall-runoff models. *Env. Mod. Soft.* **24**, 311–321.

Willems, P. 2011 Parsimonious rainfall-runoff model construction supported by time series processing and validation of hydrological extremes. *J. Hydrol.* (in revision).

Willems, P. & Berlamont, J. 2002 Accounting for the spatial rainfall variability in urban modelling applications. *Wat. Sci. Tech.* **45** (2), 105–112.

Willems, P., Molnar, P., Einfalt, T., Arnbjerg-Nielsen, K., Onof, C., Nguyen, V.-T.-V. & Burlando, P. 2012 Rainfall in the urban context: forecasting, risk and climate change. *Atmos. Res.* **103**, 1–3.

Wilson, J. W. & Brandes, E. A. 1979 Radar measurement of rainfall: a summary. *Bull. Am. Meteor. Soc.* **60**, 1048–1058.

First received 9 September 2011; accepted in revised form 5 February 2012. Available online 13 June 2012